

MODELLING TURBULENT MIXING BY RAYLEIGH–TAYLOR INSTABILITY

David L. YOUNGS

Atomic Weapons Establishment, Aldermaston, Berkshire, UK

Direct two-dimensional numerical simulation and experiments, in which small rocket motors accelerate a tank containing two fluids, have been used to investigate turbulent mixing by Rayleigh–Taylor instability at a wide range of density ratios. The experimental data obtained so far has been used to calibrate an empirical model of the mixing process which is needed to make predictions for complex applications. The model devised, which is a form of turbulence model, is based on the equations of multiphase flow. These equations describe velocity separation arising from the action of a pressure gradient on fluid fragments of different density. The dissipation arising from the drag between the fluid fragments is treated as a source of turbulence kinetic energy which is then used to define turbulent diffusion coefficients. Gradient diffusion processes are thereby included in the model.

1. Introduction

Rayleigh–Taylor instability occurs when a perturbed interface between two fluids of different density is subjected to a normal pressure gradient, Taylor [1]. If the pressure is higher in the light fluid than in the dense fluid the differential acceleration produced causes the two fluids to mix. For an overview of work published on Rayleigh–Taylor instability since [1] see the paper by Sharp [2]. One area of current interest is the effect of Rayleigh–Taylor instability on the performance of Inertially Confined Fusion capsules. A simple capsule might consist of a spherical glass shell with radius of order 100 μm filled with a deuterium/tritium gas mixture. Laser radiation (or other types of beam energy) is used to implode the capsule. The aim is to obtain sufficiently high temperatures and densities in the DT mixture for thermonuclear reactions to take place. Rayleigh–Taylor instability may occur wherever the pressure–density gradient product $\nabla p \cdot \nabla \rho$ is negative. This will arise at the start of the implosion at the ablation front between the heated and unheated glass or at the end of the implosion at the gas/glass interface. In either case instability growth tends to reduce capsule performance. Re-

cent work at AWE has investigated the latter case, mixing at fluid interfaces. Ablation front instabilities have been studied by many authors, see for example Emery et al. [3].

The term Rayleigh–Taylor instability is sometimes limited to the case when the interface between the two fluids is subjected to a finite continuous acceleration. A related process, Richtmyer–Meshkov instability [4, 5] occurs when a shock wave passes through a perturbed interface or a mixed region between fluids of different density. Both processes are important in compressible problems such as the ICF capsule implosion. The present paper will concentrate on Rayleigh–Taylor instability. The Richtmyer–Meshkov process is discussed in this volume by Brouillette [6] and Besnard et al. [7].

2. Outline of the programme

In real situations the instability will evolve from a multiple wavelength initial perturbation and turbulent mixing will occur as suggested by Youngs [8]. Direct numerical simulation of this three-dimensional process is impractical except for very

simple cases. Hence turbulence models need to be devised to make predictions for real flows. These models need to be calibrated against experimental results. Experimental studies form an essential part of the AWE programme on this topic.

The programme of work may be divided into three parts:

(a) *Direct computer simulation of the mixing processes in simple situations.* At present 2D computer codes are being used. However, in future 3D calculations will be performed. Direct computer simulation has proved to be a useful source of ideas and has played an essential role in planning the experimental programme. It also helps to understand the experimental results.

(b) *Experiments.* Definitive data on the turbulent mixing phenomena come from experimental measurements. An extensive set of experiments on the mixing of incompressible fluids by Rayleigh–Taylor instability is described by Read [9], Read and Youngs [10], Burrows, Smeeton and Youngs [11] and Smeeton and Youngs [12]. In future, experimental work at AWE will investigate the mixing of compressible gases in shock tube experiments.

(c) *Turbulence models.* The main objective of the programme is to develop turbulence models to represent the mixing processes. These models need to be calibrated against the experimental data. The turbulence models are then used to make predictions for real situations.

3. Direct numerical simulation

Work began on this study of turbulent mixing by Rayleigh–Taylor instability about ten years ago when a simple 2D finite difference incompressible code was written to calculate the growth of Rayleigh–Taylor instability at a plane boundary from a multiple wavelength initial perturbation.

The computer code solves the incompressible Navier–Stokes equations (pressure–velocity formulation) plus an equation for the fraction by volume, f_1 , of the denser fluid 1:

$$\frac{\partial f_1}{\partial t} + \text{div}(f_1 \mathbf{u}) = 0. \quad (1)$$

The fluid density is then $\rho = f_1 \rho_1 + (1 - f_1) \rho_2$. Initially the lighter fluid 2 lies above the denser fluid 1, with a body force g per unit mass acting vertically upwards. The initial volume fraction distribution is: $f_1 = 0$ for $y > \zeta(x)$ and $f_1 = 1$ for $y < \zeta(x)$ where ζ is the initial perturbation at the interface $y = 0$. This is given by

$$\zeta(x) = S \sum_n a_n \cos \frac{n\pi x}{W}$$

for rigid frictionless wall at $x = 0$ and $x = W$,

or

$$\zeta(x) = S \sum_n \left(a_n \cos \frac{2n\pi x}{W} + b_n \sin \frac{2n\pi x}{W} \right)$$

for periodic boundary conditions in the x -direction.

The a_n and b_n are random numbers chosen from a Gaussian distribution. S is a scaling factor chosen to give the required value of $\sigma = \{\langle \zeta^2 \rangle\}^{1/2}$. W is the width of the computational region in the x -direction.

The volume fraction transport equation (1) may be solved by a finite difference method which assumes a continuous variation of f_1 with position. The method of van Leer [13] is used to minimise mixing by numerical diffusion. Alternatively a front tracking method, Youngs [14], may be used to preserve a sharp interface between the two fluids. Other, more accurate, vortex methods for following Rayleigh–Taylor unstable interfaces are described by Tryggvason [15] and Kerr [16]. The front tracking method has been used for simple situations such as the growth of the instability from a single wavelength initial perturbation.

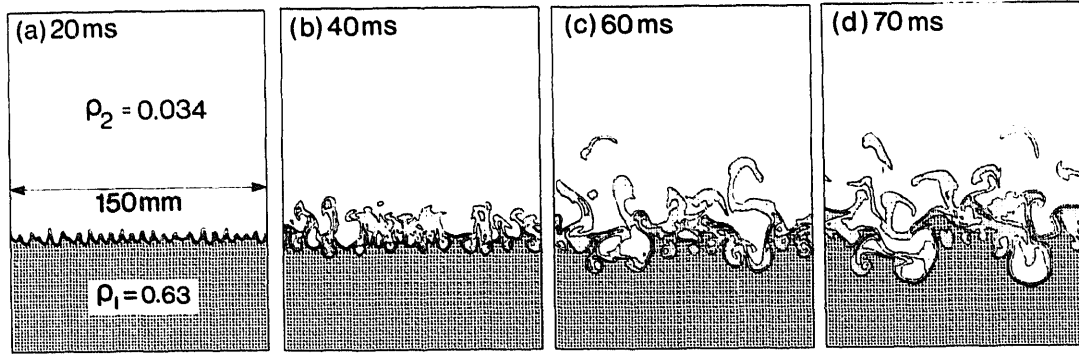


Fig. 1. Two-dimensional simulation with multiple wavelength initial perturbation. Density ratio $\rho_1/\rho_2 = 20$. Acceleration $g = 0.15$ mm/ms². Volume fraction contour levels $f_1 = 0.2, 0.5, 0.8$.

tion. It is not clear that it improves the accuracy if a multiple wavelength initial perturbation is present. In this case fine-scale (sub-zone) mixing should indeed occur due to the small scale eddies generated in the turbulent mixing region, which cannot be represented on the computational mesh. Use of the van Leer method for the transport of volume fraction and momentum introduces non-linear numerical diffusion into the calculation which plays a similar role to the subgrid eddy viscosity used in large eddy simulation of turbulent flow. The multiple wavelength calculations have used the van Leer method rather than the front tracking method.

An example is shown in fig. 1 which corresponds to the experiments described in section 4. The density ratio is $\rho_1/\rho_2 = 20$. Periodic boundary conditions are used. The initial perturbation consists of modes with wavelength in the range $W/25$ to $W/8$. The width of the computational region is $W = 150$ mm. The initial perturbation has standard deviation $\sigma = 0.025$ mm. The size of the computational mesh is 150×200 zones.

The numerical simulation shows a short wavelength perturbation of wavelength $\sim W/25$ appearing at early time. At the end of the calculation, the dominant mode has wavelength $W/2$. This has evolved from the interaction between shorter wavelength modes. It was proposed by Youngs [8] and confirmed by the experiments of Read [9] that in such circumstances the growth of the mixing zone should tend to lose memory of the

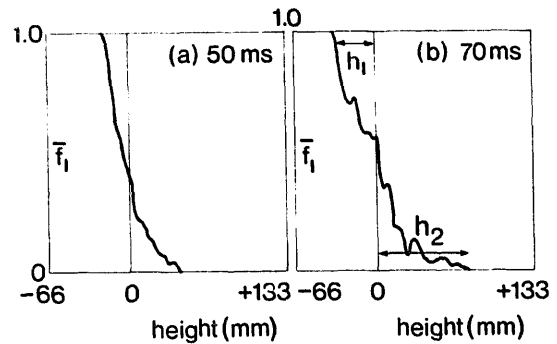


Fig. 2. Volume fraction averaged over a horizontal layer versus height, for multiple wavelength calculation.

initial conditions and that the depth to which the mixing zone penetrates the denser fluid 1 should be given by

$$h_1 = \alpha \frac{\rho_1 - \rho_2}{\rho_1 + \rho_2} g t^2. \tag{2}$$

2D numerical simulation indicated $\alpha \sim 0.04$ to 0.05 , whereas experiments suggested $\alpha \sim 0.06$ to 0.07 ;

Fig. 2 shows a plot of $\bar{f}_1 = \int f_1 dx/W$, i.e. the volume fraction averaged over a horizontal layer, versus height y , for the multiwavelength calculation. Measurements of h_1 (bubble penetration) and h_2 (spike penetration) from these plots indicate $\alpha = 0.042$ and $h_2/h_1 = 2.3$ for this calculation.

The variation of h_2/h_1 with density ratio for the single wavelength perturbation case is shown in fig. 3. The interface tracking method is used. In

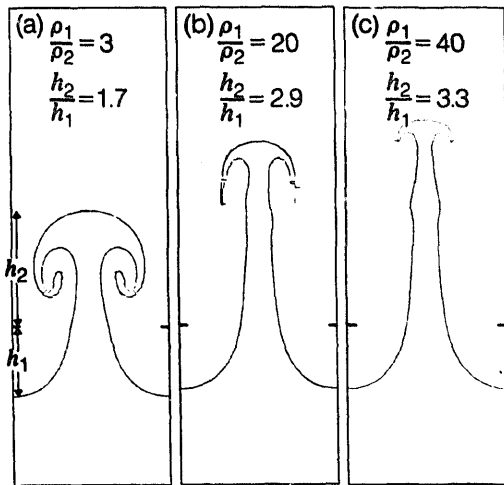


Fig. 3. Variation of h_2/h_1 with density ratio. Two-dimensional numerical simulation with single wavelength initial perturbation. Interface plots at $nt = 6$.

the absence of viscosity or other stabilising mechanisms, the growth in the linear regime of the amplitude, a , of a small perturbation of wavelength λ is given by [1] $\ddot{a} = n^2 a$, where

$$n^2 = \frac{2\pi g}{\lambda} \frac{\rho_1 - \rho_2}{\rho_1 + \rho_2}. \quad (3)$$

The initial amplitude used is $a_0 = 0.02\lambda$. For the three density ratios considered results are shown at times corresponding to the same number of exponential growth periods, i.e. $nt = 6$. h_2/h_1 is a slowly increasing function of ρ_1/ρ_2 . At $\rho_1/\rho_2 = 20$, h_2/h_1 is 2.9, a little more than the value estimated from the multiwavelength calculation, figs. 1 and 2.

The two-dimensional simulations suggested that significant instability growth should arise from small random perturbations (via mode coupling) and that the results should fit into a simple pattern, h_1 given by eq. (2) and h_2/h_1 a slowly increasing function of ρ_1/ρ_2 . As a result of the numerical simulations an experimental programme was set up to investigate the true three-dimensional behaviour. The value of the numerical simulations lies in the fact that they are an important source of ideas and a stimulus to the experimental programme, rather than in their abil-

ity to make accurate predictions of the mixing phenomena.

4. Experimental results

Experiments on the mixing of two incompressible fluids have been performed at a wide range of density ratios using the apparatus described by Read [9]. This consists of an enclosed tank containing the two fluids, initially at rest with the lighter fluid 2 on top of the denser fluid 1. The tank is then driven downwards by one or two small rocket motors. The tank is attached to two guide rods which ensure that motion of the tank is vertical. Tank accelerations are in the range $15g_0$ to $70g_0$, high enough to ensure that the effects of surface tension and viscosity are small ($g_0 = 9.8 \text{ m/s}^2$ denotes the acceleration due to gravity).

Most experiments have been carried out without any large imposed perturbations, i.e. the aim was to investigate instability growth from small random perturbations and to confirm the gt^2 growth law (2). Details of the experimental results are given in a set of three reports [10–12]. A wide range of fluid combinations has been used, for example:

Liquid / liquid:

NaI solution/hexane	$\rho_1/\rho_2 = 3$,
NaI solution/water	$\rho_1/\rho_2 = 1.8$.

Liquid / gas:

alcohol/air (1 bar)	$\rho_1/\rho_2 = 700$,
pentane/SF ₆ (up to 10 bar)	$\rho_1/\rho_2 = 8$ to 30.

Some of the latest experiments [12] used a combination of a liquid and a compressed dense gas, SF₆. This enabled density ratios in the range 8 to 30 to be used where computer simulation – see section 3 – had indicated that there was uncertainty in the depth to which spikes at heavy fluid would penetrate the lighter fluid. Photographs for two examples of the pentane/compressed SF₆ experiments are shown in fig. 4 ($\rho_1/\rho_2 = 8.5$) and fig.

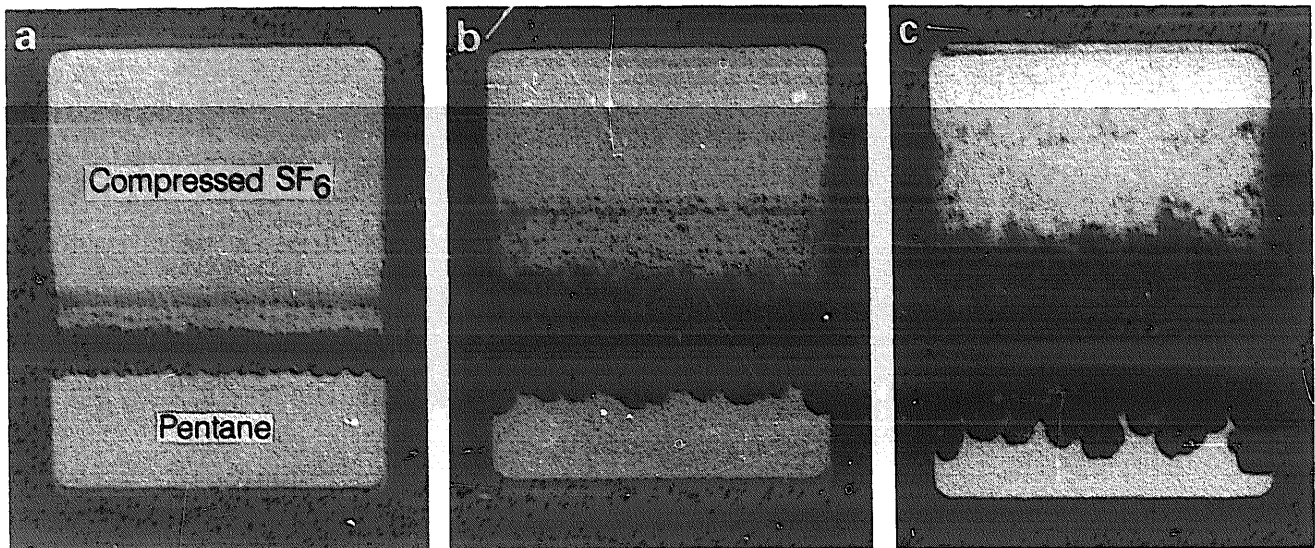


Fig. 4. Pentane/compressed SF₆ experiment. Density ratio $\rho_1/\rho_2 = 8.5$. Acceleration $g = 15g_0$. (a) 32.8 ms. (b) 53.3 ms. (c) 73.7 ms.

5 ($\rho_1/\rho_2 = 29.1$). The width of the tank in these and subsequent experiments is $W = 150$ mm. As the two fluids have very different refractive indices, the mixed region appears black on the backlit photographs. The photographs clearly show the increase in bubble size as time proceeds. The presence of the meniscus at the start of the experiment results in a thin film of liquid climbing the tank walls. Also large bubbles form in the tank

corners where the effect of the meniscus is greatest. These effects are ignored when measurements of growth rates are made; h_1 and h_2 are measured on the darkest region in the centre of the tank.

Plots of h_1 against $(\rho_1 - \rho_2)/(\rho_1 + \rho_2)gt^2$ for these two experiments are shown in fig. 6. Reasonably good linear correlations are obtained, though for the higher density ratio experiment there is some slowing down of the growth rate at late time

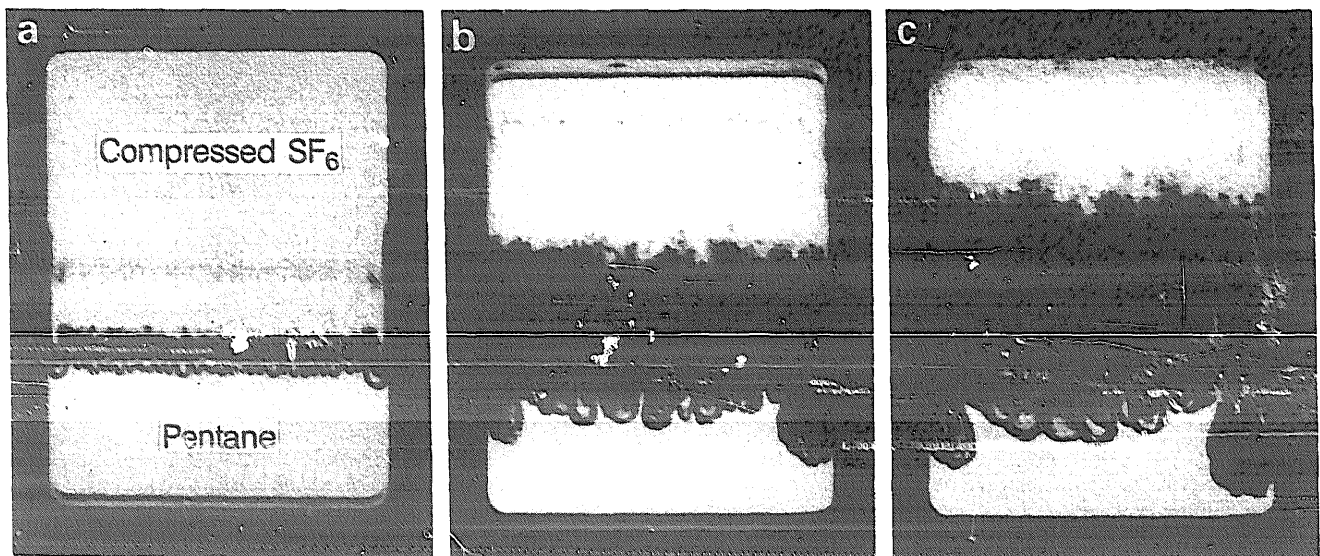


Fig. 5. Pentane/compressed SF₆ experiment. Density ratio $\rho_1/\rho_2 = 29.1$. Acceleration $g = 15g_0$. (a) 33.5 ms. (b) 56.9 ms. (c) 67.3 ms.

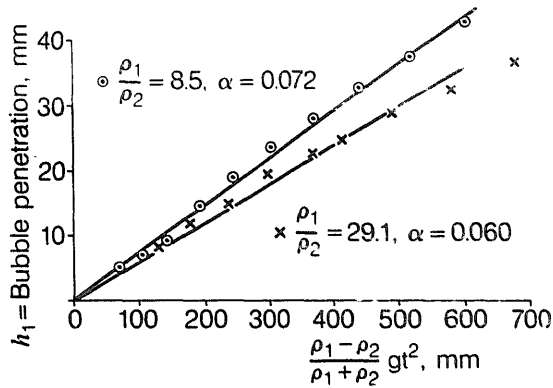


Fig. 6. Bubble penetration versus scaled acceleration distance for two pentane/compressed SF₆ experiments.

which may be due to the dominance of the large corner bubbles at this stage. The values of α for these two experiments are 0.072 and 0.060.

α has been measured for about 50 of the experiments described in refs. [10–12]. The values obtained lie in the range 0.050 to 0.077. There is no noticeable variation with density ratio. Some of the experiments were of better quality than others. If this is taken into account, the recommended value is $\alpha = 0.06$ for all density ratios.

The variation of h_2/h_1 with density ratio is shown in fig. 7. As predicted by the numerical simulations h_2/h_1 is a slowly increasing function of ρ_1/ρ_2 . At $\rho_1/\rho_2 = 20$, the experimental results give $h_2/h_1 = 2.0$, a little less than the value of 2.3 indicated by the multiwavelength numerical simulation, fig. 1.

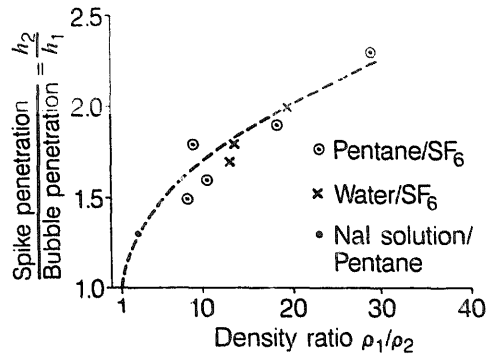


Fig. 7. Experimental variation of h_2/h_1 with density ratio.

In some experiments the fluids used were CaCl₂ solution and hexane with the CaCl₂ concentration adjusted so that the two fluids had the same refractive index. The density ratio obtained is $\rho_1/\rho_2 = 1.73$. The CaCl₂ solution is dyed and the backlighting made as uniform as possible. The fluids then act as pure absorbers of the backlight and the film density, d , on the photographic negative may be related to the amount of dyed fluid. The dye level is chosen so that d varies linearly with f_1 in calibration tests. Then for the experiments

$$f_1 = \frac{d_{\text{max}} - d}{d_{\text{max}} - d_{\text{min}}},$$

where d_{max} is the film density at the top of the tank (pure fluid 2) and d_{min} is the film density at the bottom of the tank (pure fluid 1). Fig. 8 shows

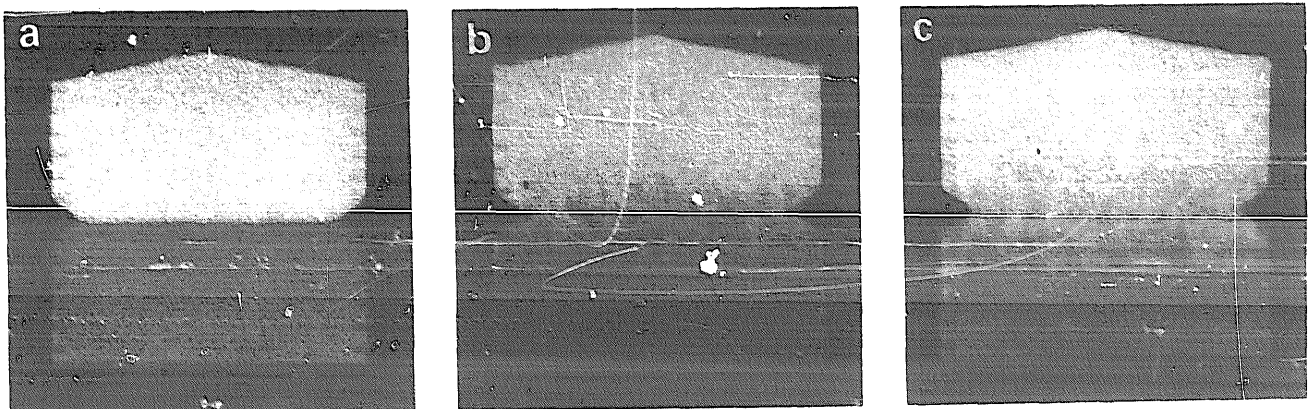


Fig. 8. Experiment using fluids with matched refractive indices. CaCl₂ solution (dyed)/hexane (clear). Density ratio $\rho_1/\rho_2 = 1.73$. Acceleration $g = 43g_0$. (a) 0 ms. (b) 63.0 ms. (c) 73.9 ms.

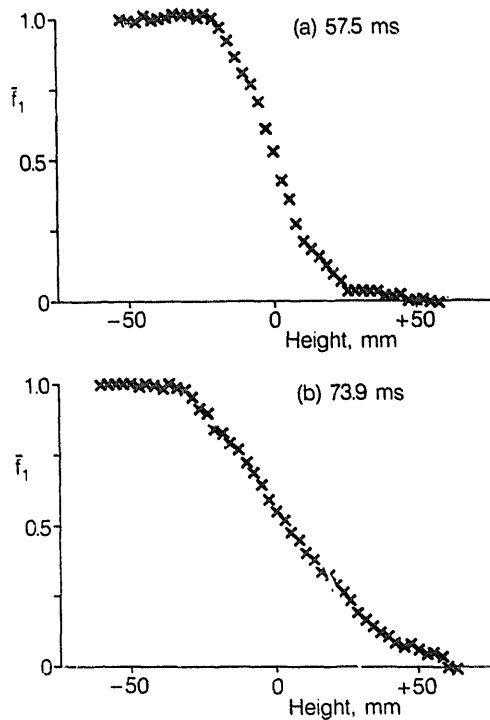


Fig. 9. Volume fraction averaged over a horizontal layer versus height for the experiment shown in fig. 8.

photographs for one of the matched refractive index experiments. Fig. 9 shows plots of \bar{f}_1 , i.e. f_1 averaged over a horizontal layer, versus height. The shape obtained is in reasonable agreement with that expected from 2D numerical simulation. However, the experimental profile should be regarded as approximate because of the difficulty in achieving perfectly uniform backlighting and in matching the refractive indices exactly.

For the two experiments described in [12] the tank was first accelerated as usual and then, when the rocket motor had burnt out, was decelerated by springs. In the final stage the tank moved vertically upwards with near constant velocity. These experiments also used the CaCl_2 solution/hexane combination. The bubble penetration h_1 , shown in fig. 13(a), was deduced from the \bar{f}_1 profile. h_1 was measured to the point where $\bar{f}_1 = 0.95$. During the acceleration phase h_1 increases as expected. During the deceleration phase h_1 decreases, i.e. partial de-mixing occurs. In the final coasting phase the mixed region grows again. It is

shown in the next section how the late time behaviour may be modelled by a combination of pressure gradient and turbulent diffusion effects.

Some experiments described in [11, 12] used three layers of liquid, carbon tetrachloride/NaCl solution/hexane, with densities $\rho_1 > \rho_2 > \rho_3$. The density of the intermediate layer was chosen so that $\rho_2 = \sqrt{(\rho_1 \rho_3)}$, i.e. the Atwood number was the same at the two interfaces. The initial thickness of the intermediate layer Δ varied from 5 to 20 mm. However, it proved difficult to obtain good results with $\Delta = 5$ mm; the meniscus on the top and bottom of the layer appeared to affect the results. The aim of these experiments was to quantify the reduction in the mixing of fluids 1 and 3 due to the intermediate layer. In order to obtain results in a non-dimensional form δ/Δ is plotted (see fig. 16(a)) against $(\rho_1 - \rho_2)/(\rho_1 + \rho_2)gt^2/\Delta$ where the width of the mixed region δ (which equals Δ at $t = 0$) is the distance between the boundary of the unmixed fluid 1 and the boundary of the unmixed fluid 3. At early times the rate of growth of δ is about half that expected without the intermediate layer. This is consistent with the reduced initial Atwood number. However, even when $\delta \sim 5\Delta$ long after the intermediate layer is fully mixed the growth rate appears to be significantly reduced by the effect of the intermediate layer.

In several experiments the tank and guide rods were inclined at an accurately measured angle, θ , to the vertical. The acceleration g remained parallel to the tank sides and the initial interface was inclined at an angle θ to the direction of acceleration. The inclination of the initial interface results in a gross overturning motion in addition to the fine scale mixing. This gives a flow which is on average two-dimensional from precisely known initial conditions and provides data for testing future two-dimensional versions of the turbulence model described in the next section. Results for two such experiments are shown in figs. 10 ($\rho_1/\rho_2 = 3$) and 11 ($\rho_1/\rho_2 = 20$). At $\rho_1/\rho_2 = 3$ a large bubble of fluid 2 penetrates the heavier fluid at the right-hand side of the tank. A similar structure forms on the left-hand side of the tank. This grows

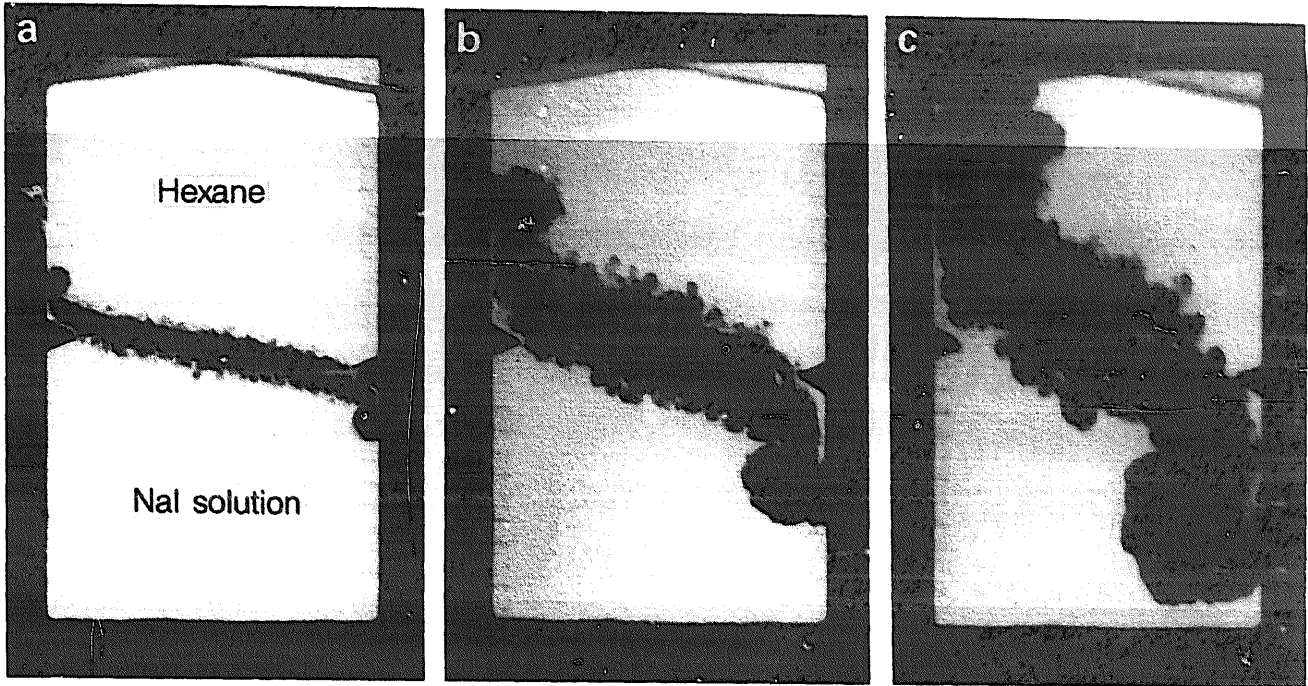


Fig. 10. NaI solution/hexane experiment. Rig tilted by $5^{\circ}46'$. Density ratio $\rho_1/\rho_2 = 2.9$. Acceleration $g = 35g_0$. (a) 35.7 ms. (b) 54.9 ms. (c) 71.1 ms.

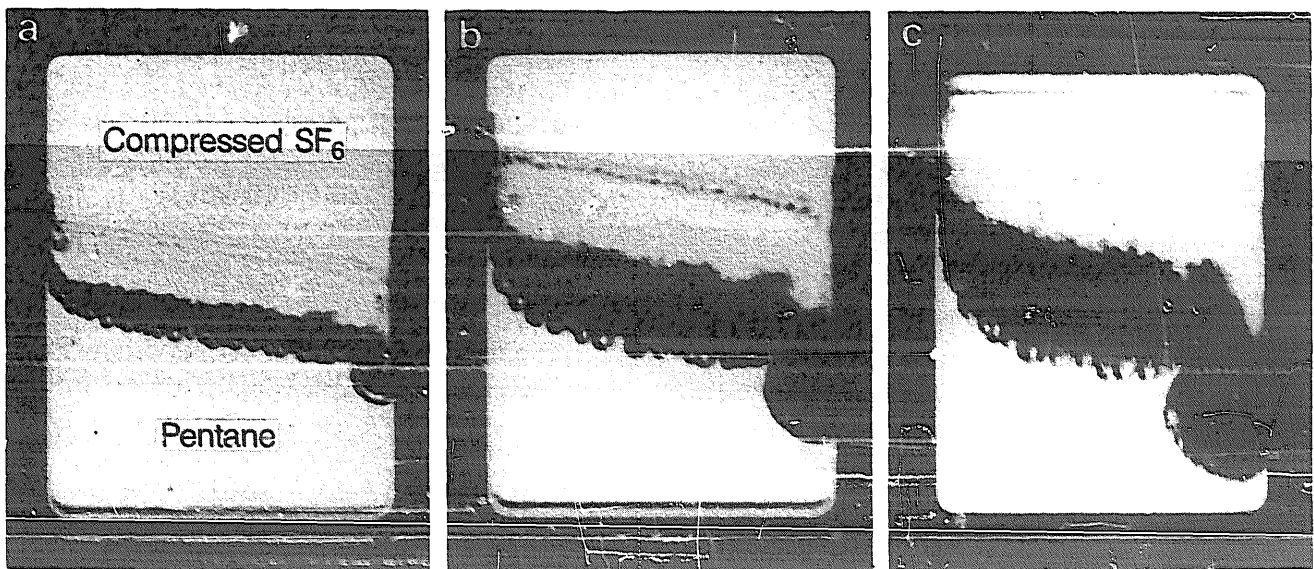


Fig. 11. Pentane/compressed SF_6 experiment. Rig tilted by $5^{\circ}9'$. Density ratio $\rho_1/\rho_2 = 19.6$. Acceleration $g = 16g_0$. (a) 31.2 ms. (b) 42.3 ms. (c) 52.9 ms.

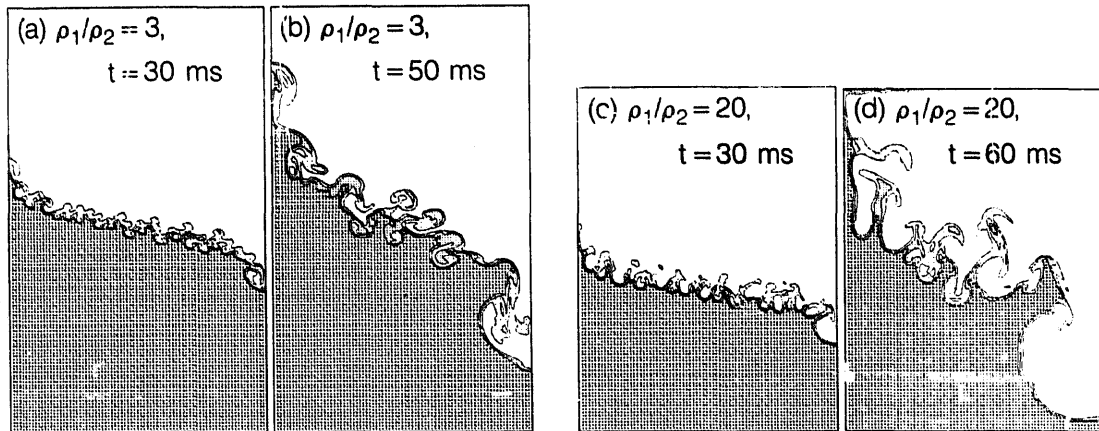


Fig. 12. Two-dimensional numerical solution of the tilted-rig experiments. Volume fraction contour levels, $f_1 = 0.2, 0.5, 0.8$.

a little faster. At $\rho_1/\rho_2 = 20$, the behaviour is significantly different. In this case a thin spike of fluid 1 forms at the left-hand side of the tank. Results of two-dimensional numerical simulation of these two experiments are shown in fig. 12. Rigid frictionless walls were used at $x = 0$ and $x = W$. The initial perturbation consisted of a combination of cosine modes with $n = 31$ to 50 and $\sigma = 0.025$ mm (see section 3), superimposed on the tilted interface. The simulations reproduce the behaviour of the observed features at the sides of the tank. This shows that neither wall friction nor the presence of the meniscus has a major effect on the development of these features. The fine scale mixing in the centre of the tank appears to be underestimated in the simulations. It is likely that three-dimensional simulations would be needed to calculate this correctly.

5. Turbulence models

5.1. The model equations

Turbulence models are needed to predict the average mixing behaviour in flows that are on average one- or two-dimensional. The approach to the construction of the turbulence model is guided by the experimental behaviour. The photographs in figs. 4 and 5 clearly show bubbles of gas pene-

trating the denser liquid. At any given time there appears to be a characteristic bubble size which increases as the mixed region develops. Instead of using closure laws for fluctuating quantities, as is done in many turbulence models, the present model is based on representing the dynamics of the observed structures in the mixed region (bubbles of light fluid or drops of dense fluid). The need to model the motion of bubbles or drops in a pressure gradient suggests using the equations of multiphase flow. A simple two-phase flow model for Rayleigh–Taylor instability was described by Youngs [3]. The present paper considers the extension to many fluids and the addition of extra physics. Two-fluid turbulence models have been widely used by Spalding and were applied to mixing of fluids by Rayleigh–Taylor instability in [17]. Andrews [18] has considered the extension of a simple two-fluid model for Rayleigh–Taylor instability to two dimensions. Alternative approaches for the Richtmyer–Meshkov case are described in these proceedings by Besnard et al. [7].

The present multiphase flow model represents the following effects:

- (i) differential acceleration induced by the pressure gradient on fluid fragments of different densities;
- (ii) drag between fluid fragments, proportional to velocity difference squared;

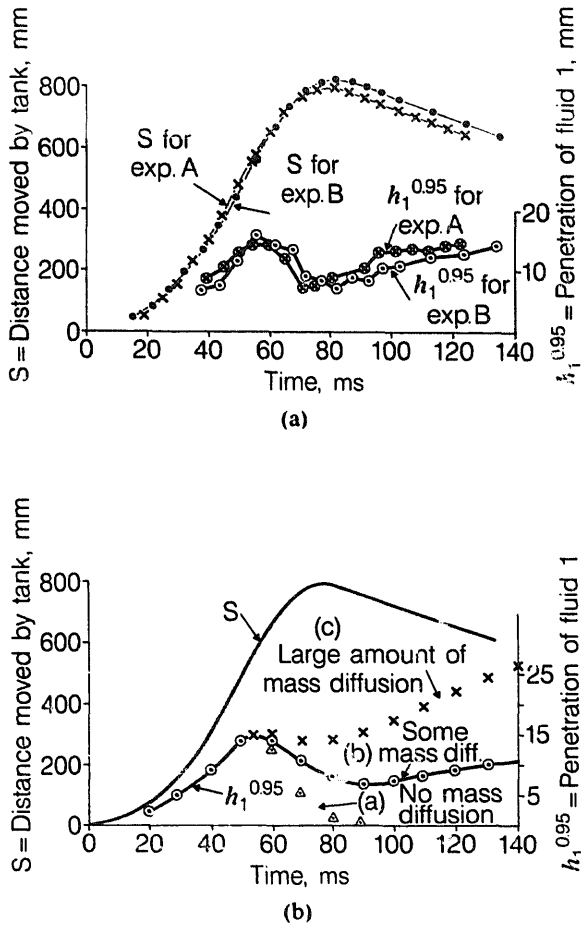


Fig. 13. Acceleration/deceleration experiments: (a) observed results, (b) turbulence model predictions.

- (iii) added mass;
- (iv) increase of length scale (bubble or drop radius) in proportion to the width of the mixed region.

However, these effects do not include all the important physics. Inter-fluid drag provides a source of turbulence kinetic energy. This leads to mixing by turbulent diffusion which is needed to explain the late stage mixing observed in the acceleration/deceleration experiments, fig. 13(a). It is well known – see for example Jones and Prosperetti [19] – that many simple multiphase flow models give rise to an ill-posed equation set. It is suggested here that the inclusion of turbulent diffusion terms should alleviate this problem, as well as improving the physics. In some simple situations it can be shown that the method of including

turbulent diffusion terms described here gives rise to an equation set which has stable solutions. The analysis is given in the appendix.

The extra effects included in the model are:

- (i) a turbulence kinetic energy equation;
- (ii) transport of mass by turbulent diffusion;
- (iii) transport of momentum by turbulent diffusion (Reynolds stress);
- (iv) length scale diffusion.

For simplicity, the use of the model for one-dimensional planar incompressible flows is described. The model has been applied to one-dimensional compressible flows. In the model the mean values of the volume fraction for fluid r (f_r), the density of fluid r (ρ_r), the velocity of fluid r (u_r), the length scale (L) and the turbulence kinetic energy (k) are functions of distance (x) and time (t). The model equations are as follows.

Mass transport:

$$\frac{\partial}{\partial t} (\rho_r f_r) + \frac{\partial}{\partial x} (\rho_r f_r u_r) = 0. \quad (4)$$

Momentum transport:

$$\begin{aligned} \frac{\partial}{\partial t} (\rho_r f_r u_r) + \frac{\partial}{\partial x} (\rho_r f_r u_r^2) \\ = -f_r \frac{\partial p}{\partial x} + \sum_s D_{rs} + \sum_s M_{rs} - m_r \frac{\partial R}{\partial x}. \end{aligned} \quad (5)$$

Length scale:

$$\frac{\partial L}{\partial t} + u_L \frac{\partial L}{\partial x} = S + \frac{\partial}{\partial x} \left(D_L \frac{\partial L}{\partial x} \right). \quad (6)$$

Turbulence kinetic energy:

$$\frac{\partial}{\partial t} (\rho k) + \frac{\partial}{\partial x} (\rho \tilde{u} k) = \frac{\partial}{\partial x} \left(\rho D_k \frac{\partial L}{\partial x} \right) + S_k - \epsilon. \quad (7)$$

Many of the terms appearing in eqs. (4) to (7) require further explanation. \tilde{u} denotes the mass weighted mean velocity.

M_{rs} represents the added mass for fluid r due to fluid s . This is given by

$$\left. \begin{aligned} M_{rs} &= -0.5\rho_{rs}f_r f_s \left(\frac{D_r u_r}{Dt} - \frac{D_s u_s}{Dt} \right), \text{ where} \\ \frac{D_r u_r}{Dt} &= \frac{\partial u_r}{\partial t} + u_r \frac{\partial u_r}{\partial x} \\ \rho_{rs} &= (f_r \rho_r + f_s \rho_s) / (f_r + f_s). \end{aligned} \right\} \quad (8)$$

is the acceleration of fluid r and

$$\rho_{rs} = (f_r \rho_r + f_s \rho_s) / (f_r + f_s).$$

This is an extension to many fluids of one of the formulae for two-fluid flow analysed in [19]. The coefficient 0.5 is chosen to give the correct added mass for isolated spherical particles of fluid r surrounded by fluid s .

D_{rs} denotes the drag on fluid r due to fluid s and is given by

$$\begin{aligned} D_{rs} &= -c_1 \frac{\rho_{rs} f_r f_s}{L} |u_r - u_s - w_r + w_s| \\ &\quad \times (u_r - u_s - w_r + w_s). \end{aligned} \quad (9)$$

The drag coefficient c_1 is obtained by matching experimental data, as will be explained in the next section. w_r is the value of $u_r - \bar{u}$ expected if mixing is entirely due to turbulent diffusion. \bar{u} denotes the volume weighted mean velocity. In that case mass flow is given by

$$\frac{\partial \rho}{\partial t} + \frac{\partial}{\partial x} (\rho \bar{u}) = \frac{\partial}{\partial x} \left(D \frac{\partial \rho}{\partial x} \right)$$

with mean density $\rho = \sum f_r \rho_r$. This can be interpreted as fluid r mass flux:

$$\rho_r f_r u_r = \rho_r f_r \bar{u} - D \frac{\partial}{\partial x} (f_r \rho_r),$$

whence

$$w_r = - \frac{D}{f_r \rho_r} \frac{\partial}{\partial x} (f_r \rho_r)$$

with D = turbulent diffusion coefficient.

When the drag coefficient $c_1 \rightarrow \infty$, $u_r - u_s = w_r - w_s$ as required.

The source term in the length scale equation (6) is

$$S_L = \sum_{r>s} f_r f_s \left\{ \frac{2\rho_{rs}}{\rho_r + \rho_s} \right\}^{1/2} (u_s - u_r) / \sum_{r>s} f_r f_s. \quad (10)$$

The fluids are numbered $r = 1, 2, 3, \dots$ in order of increasing initial position. Then $S_L > 0$ if the fluids are mixing and $S_L < 0$ if the fluids are de-mixing.

For two fluids

$$S_L = \left\{ \frac{2\rho}{\rho_1 + \rho_2} \right\}^{1/2} (u_1 - u_2).$$

This form is chosen to give an approximately uniform length scale, proportional to the width of the mixed region. Eq. (10) is simply a plausible extension of the two-fluid formula.

For the two-fluid case the advection velocity in the length scale equation is

$$u_L = \bar{u} + (f_2 - f_1)(u_1 - u_2).$$

This formulation, due to Andrews [18], transports the length scale away from the centre of the mixed region and was found to improve the stability of the solution. For the multifluid case u_L is obtained by a plausible extension of the two-fluid formula:

$$u_L = \bar{u} + \sum_{r>s} f_r f_s (f_r - f_s) (u_s - u_r) / \sum_{r>s} f_r f_s.$$

The term $-m_r \partial R / \partial x$ in the momentum transport equation, where $m_r = f_r \rho_r / \rho$ is the fluid r mass fraction, represents the effect of the Reynolds stress. The use of the mass fraction in this term will be explained later. As in turbulent diffusion models such as the (k, ϵ) model, see for example Leith [20], the Reynolds stress in one-dimensional planar geometry is given by

$$R = \frac{2}{3} \rho k - \frac{4}{3} \mu_t \frac{\partial \bar{u}}{\partial x},$$

with

$$\mu_t = \rho k^{1/2} l_t,$$

l_t = turbulence length scale.

The turbulence kinetic energy equation (7) is also the same as that used in turbulent diffusion models. The dissipation rate is

$$\epsilon = 0.09 \frac{\rho k^{3/2}}{l_t}.$$

The coefficient 0.09 is an appropriate value for turbulent shear flow models, see Launder and Spalding [21]. However, it should be pointed out that there are no experimental measurements of the dissipation of k in Rayleigh–Taylor mixing. The turbulent diffusion coefficients D and D_k are the same as for turbulent shear flow [21], i.e. $D = 2k^{1/2}l_t$ (mass diffusion) and $D_k = k^{1/2}l_t$ (k -diffusion). In the length scale equation $D_L = 2k^{1/2}l_t$ is used.

The source term in the turbulent kinetic equation (7) is

$$S_k = \sum_{r < s} (u_s - u_r)(M_{rs} + D_{rs}) - R \frac{\partial \tilde{u}}{\partial x}.$$

The turbulence length scale is assumed to be proportional to the fragment size L . Two model constants now remain which need to be chosen to fit data on Rayleigh–Taylor mixing. These are

c_1 = drag coefficient, determines the overall mixing rate,

$c_2 = l_t/L$, determines the relative importance of turbulent diffusion and pressure gradient effects.

In order to check that turbulent diffusion effects have been incorporated in a plausible manner it is worthwhile examining a simple limiting case, the drift-flux approximation for two-fluid mixing. This is valid when the inertial effects on the velocity separation $u_1 - u_2$ are negligible and, following

Travis et al. [22], may be obtained by setting

$$\frac{D_1 u_1}{D t} = \frac{D_2 u_2}{D t}.$$

The added mass terms vanish and equating the fluid accelerations gives

$$\begin{aligned} -\frac{1}{\rho_1} \frac{\partial p}{\partial x} + \frac{D_{12}}{\rho_1 f_1} + \frac{1}{\rho} \frac{\partial R}{\partial x} \\ = -\frac{1}{\rho_2} \frac{\partial p}{\partial x} + \frac{D_{21}}{\rho_2 f_2} + \frac{1}{\rho} \frac{\partial R}{\partial x}, \end{aligned}$$

with

$$\begin{aligned} D_{12} &= -D_{21} \\ &= -\frac{c_1 \rho_1 f_1 f_2}{L} |u_1 - u_2 + w_1 - w_2| \\ &\quad \times (u_1 - u_2 + w_1 - w_2), \end{aligned}$$

whence

$$\begin{aligned} u_1 - u_2 &= S \left\{ \frac{L}{c_1} \left| \frac{\rho_1 - \rho_2}{\rho^2} \frac{\partial p}{\partial x} \right| \right\}^{1/2} + w_1 - w_2 \\ &= \text{pressure diffusion term} \\ &\quad + \text{gradient diffusion term,} \\ S &= \text{sign} \left\{ (\rho_1 - \rho_2) \frac{\partial p}{\partial x} \right\}. \end{aligned}$$

A plausible result is obtained. Velocity separation is due to a combination of pressure diffusion and gradient diffusion effects. As a result of using the mass fraction m_r in the Reynolds stress term in eq. (5), the Reynolds stress terms cancel and the velocity separation due to turbulent diffusion is, as required, given by the $w_1 - w_2$ term.

There is one major omission in the present model. In many of the applications, such as the ICF implosion referred to in the introduction, the fluids involved will be miscible and, as a result of the presence of small scale eddies in the turbulent mixing zone, will to some extent mix at a molecular or atomic level. This will have many effects. The density differences on which the pressure gra-

dient acts will be reduced. Mixing at a molecular level will inhibit the de-mixing which will occur if the acceleration changes from the unstable to the stable direction. It is planned to model these effects by an exchange of mass between the fluids. However, the model would need to be calibrated against experiment and there is at present no observed data on the degree of molecular or fine-scale mixing in Rayleigh–Taylor unstable flows.

5.2. Application of the model

The observed growth rate, eq. (2) with $\alpha = 0.06$, may be matched by adjusting c_1 or c_2 . Three possible ways are:

(a) no mass diffusion ($D = 0$)

$$c_1 = 6.83 - 2.3 \left| \frac{\rho_r - \rho_s}{\rho_r + \rho_s} \right|, \quad c_2 = 0.075;$$

(b) some mass diffusion ($D = 2k^{1/2}l_1$)

$$c_1 = 11.5 - 3.5 \left| \frac{\rho_r - \rho_s}{\rho_r + \rho_s} \right|, \quad c_2 = 0.075;$$

(c) large amount of mass diffusion ($D = 2k^{1/2}l_1$)

$$c_1 = 23.2 - 6.3 \left| \frac{\rho_r - \rho_s}{\rho_r + \rho_s} \right|, \quad c_2 = 0.15.$$

Results obtained for the acceleration/deceleration experiments, described in section 4, are shown in fig. 13. The coefficient set (a) (no mass diffusion) gives too much de-mixing and no late time growth of the mixed region. For the coefficient set (c) (large amount of mass diffusion) there is little de-mixing and too much late time growth. The coefficient set (b) (with the intermediate amount of mass diffusion) agrees reasonably well with the observed data. This shows that the model is able to give the correct qualitative behaviour for these experiments. However, it should be pointed out that the observed de-mixing may well have been affected by the fact that immiscible liquids were used. Also, the behaviour of the model would be somewhat different if molecular mixing had been included as suggested in section 5.1.

The model, with coefficient set (b), has been applied to two simple problems which correspond to some of the experimental situations. The initial geometries for the two problems are as follows:

(a) *Two fluid problem*

$$\text{fluid 1: } 0 < x < 100 \text{ mm} \quad \rho = 1 \text{ mg/mm}^3;$$

$$\text{fluid 2: } 100 \text{ mm} < x < 200 \text{ mm} \quad \rho = 3 \text{ mg/mm}^3.$$

The initial pressure gradient is chosen to give an acceleration of

$$-\frac{1}{\rho} \frac{\partial p}{\partial x} = g = 0.5 \text{ mm/ms}^2,$$

which corresponds to that attained in some of the rocket-driven experiments. The problem has been calculated on a one-dimensional compressible Lagrangian code with boundary conditions $p = 400$ kPa (left-hand boundary) and $p = 200$ kPa (right-hand boundary). The equation of state used for both fluids is $p = (\frac{2}{3})\rho\epsilon$. The fluids are almost incompressible and the undisturbed region moves with acceleration close to g .

(b) *Three fluid problem*

This is the two fluid problem with an intermediate layer added:

$$\text{fluid 1: } 0 < x < 100 \text{ mm} \quad \rho = 1 \text{ mg/mm}^3;$$

$$\text{fluid 2: } 100 \text{ mm} < x < 110 \text{ mm} \quad \rho = \sqrt{3} \text{ n.g/mm}^3;$$

$$\text{fluid 3: } 110 \text{ mm} < x < 210 \text{ mm} \quad \rho = 3 \text{ mg/mm}^3.$$

The equation of state, pressure on the right hand boundary and acceleration g are the same as for the two-fluid problem.

Calculations have been carried out with an initial mesh size $\Delta x = 5$ mm for problem (a) and $\Delta x = 5$ mm in fluids 1 and 3, $\Delta x = 2.5$ mm in the

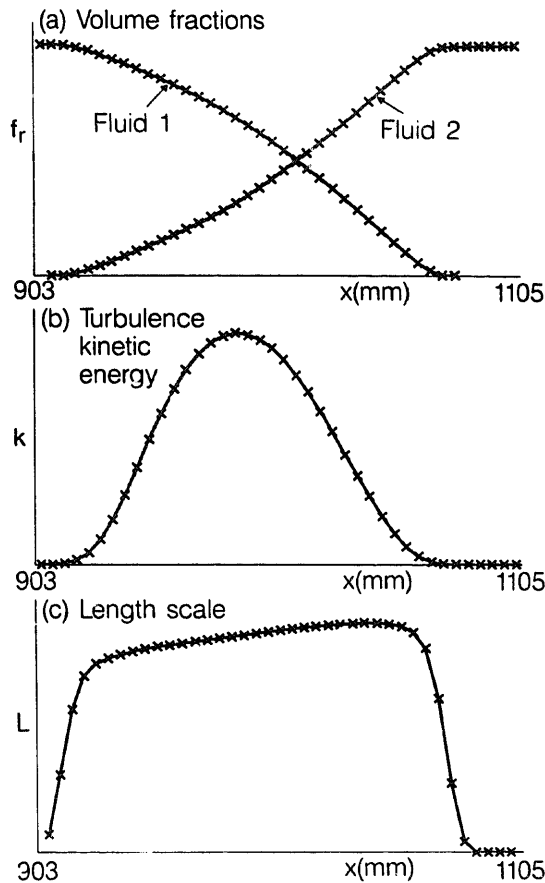


Fig. 14. Turbulence model results for the two-fluid problem at $t = 60$ ms.

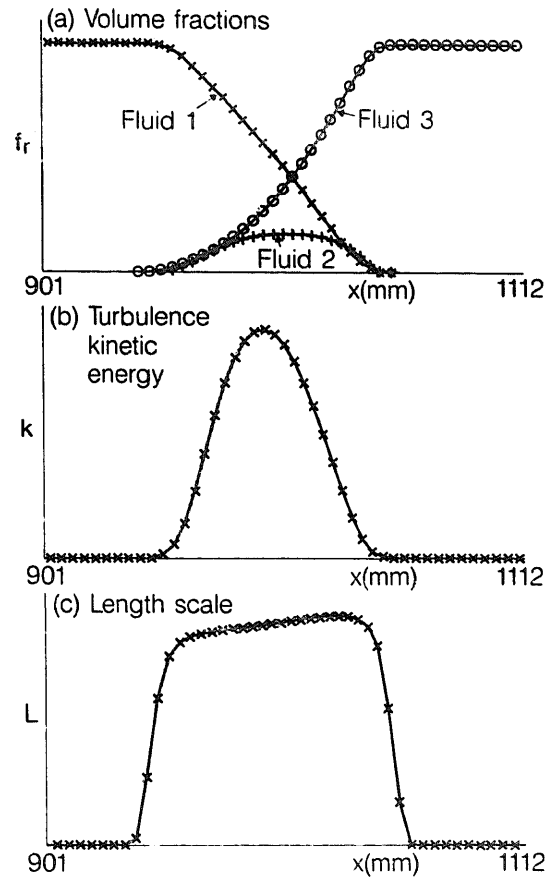


Fig. 15. Turbulence model results for the three-fluid problem at $t = 60$ ms.

thin intermediate layer for problem (b). Plots of f_r , L and k against x are shown in figs. 14 and 15. Fig. 16(b) shows a plot of δ , the width of the mixed region against gt^2 , for problems (a) and (b). δ is defined as the distance between the points where $f_1 = 0.95$ and $f_2 = 0.95$ (problem (a)) or $f_1 = 0.95$ and $f_3 = 0.95$ (problem (b)). For problem (a) δ varies linearly with gt^2 . However, the straight line does not pass through the origin. Extrapolating back to $t = 0$ gives $\delta \sim 1.2 \Delta x$ at $t = 0$. This slight overshoot is due to numerical diffusion in the solution of the volume fraction transport equation. The method used for volume fraction transport is derived from the high-order monotonic advection method of van Leer [13]. If first order, upwind differencing had been used the numerical error would have been far greater.

The effect of the intermediate layer on the growth rate of the mixed region agrees well with the experimental results shown in fig. 16(a).

6. Conclusions

Direct numerical simulation gives insight into the way fluids mix by Rayleigh–Taylor instability in idealised situations. Simple laboratory experiments have confirmed the picture of the mixing process indicated by numerical simulation and have provided good estimates of the growth rate of the turbulent mixing zone at a wide range of density ratios.

In order to make predictions for real applications an empirical model of the mixing processes

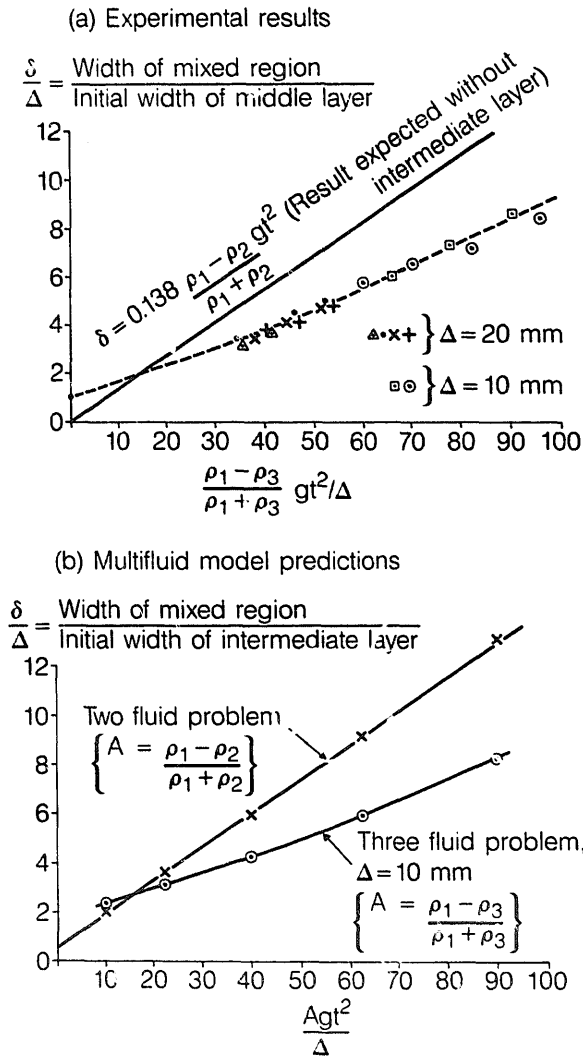


Fig. 16. Width of mixed region versus scaled acceleration distance for two-fluid and three-fluid experiments: (a) observed results, (b) turbulence model predictions.

needs to be devised. It has been shown that the multiphase flow equations with turbulent diffusion terms added provide a suitable framework for such a model. The equations model the mixing of fluids arising from the action of a pressure gradient on fluid fragments of different densities, as well as mixing by gradient diffusion. The empirical model needs to be calibrated against observed data. The experimental results obtained so far provide a good basis. However, there are some gaps in the measurements such as the proportion of the turbulence kinetic energy which is dissi-

pated into heat and the extent to which the fluids mix at a molecular level. Several research laboratories are at present investigating the mixing of gases of different densities in shock tube experiments. The data obtained from these experiments will play an essential role in validating the model in compressible situations.

Appendix

Stability of the model equations

It is well known (see for example Jones and Prosperetti [19]) that the multiphase flow equations, described in section 5.1, with turbulent diffusion effects omitted, give rise to unstable solutions. By using the same type of perturbation analysis as described in [19], it is shown here that the addition of turbulent diffusion terms removes the problem in a simple two-fluid case. Reynolds stress terms, which have negligible effect on the one-dimensional incompressible problems considered here, are omitted as they complicate the analysis. The equations considered are:

Volume fraction:

$$\frac{\partial f_r}{\partial t} + \frac{\partial}{\partial x} (f_r u_r) = 0. \tag{A.1}$$

Acceleration:

$$f_r \rho_r \frac{D_r u_r}{D t} = -f_r \frac{\partial p}{\partial x} + M_{rs} + D_{rs} + f_r \rho_r g, \tag{A.2}$$

with $r = 1, 2$ and $s \neq r$.

The added mass terms are

$$M_{12} = -M_{21} = -c_a f_1 f_2 \rho \left(\frac{D_1 u_1}{D t} - \frac{D_2 u_2}{D t} \right),$$

where $c_a = 0.5$ is the added mass coefficient, and

the drag terms are

$$\begin{aligned}
 D_{12} &= -D_{21} \\
 &= -\frac{c_1 f_1 f_2 \rho}{L} \left| u_1 - u_2 + \frac{D}{f_1 f_2} \frac{\partial f_1}{\partial x} \right| \\
 &\quad \times \left(u_1 - u_2 + \frac{D}{f_1 f_2} \frac{\partial f_1}{\partial x} \right).
 \end{aligned}$$

Elimination of the pressure gradient from the two acceleration equations (A.2) gives

$$\begin{aligned}
 (\rho_1 + c_a \rho) \frac{D_1 u_1}{Dt} - (\rho_2 + c_a \rho) \frac{D_2 u_2}{Dt} \\
 = (\rho_1 - \rho_2) g - \frac{c_1 \rho}{L} \left| u_1 - u_2 + \frac{D}{f_1 f_2} \frac{\partial f_1}{\partial x} \right| \\
 \times \left(u_1 - u_2 + \frac{D}{f_1 f_2} \frac{\partial f_1}{\partial x} \right). \tag{A.3}
 \end{aligned}$$

A gravitational force, g , chosen so that $(\rho_1 - \rho_2)g > 0$, is added so that a non-trivial uniform steady-state solution exists with

$$\begin{aligned}
 f_1 &= f_1^0, \\
 f_2 &= f_2^0, \\
 u_1 - u_2 &= u_1^0 - u_2^0 = \left(\frac{\rho_1 - \rho_2}{c_1 \rho} g L \right)^{1/2},
 \end{aligned}$$

where f_1^0, f_2^0, u_1^0 and u_2^0 are constants. The length scale L is also assumed to be constant. A small perturbation to the solution is considered:

$$\begin{aligned}
 f_r &= f_r^0 + \hat{f}_r e^{i(\omega t + kx)}, \\
 u_r &= u_r^0 + \hat{u}_r e^{i(\omega t + kx)}.
 \end{aligned}$$

Substitution in eqs. (A.1) and (A.3), with terms linear in \hat{f}_r and \hat{u}_r only being retained, gives

$$\begin{aligned}
 A_1 \hat{f}_1 + k f_1^0 \hat{u}_1 &= 0, \\
 A_2 \hat{f}_2 + k f_2^0 \hat{u}_2 &= 0, \\
 \rho_1^* i A_1 \hat{u}_1 - \rho_2^* i A_2 \hat{u}_2 \\
 &= -\frac{2c_1 \rho^0}{L} |u_1^0 - u_2^0| \left(\hat{u}_1 - \hat{u}_2 + \frac{i k D^0 \hat{f}_1}{f_1^0 f_2^0} \right),
 \end{aligned}$$

with

$$\begin{aligned}
 A_r &= \omega + k u_r^0, \\
 \rho_r^* &= \rho_r + c_a \rho^0, \\
 \hat{f}_1 + \hat{f}_2 &= 0.
 \end{aligned}$$

Elimination of \hat{f}_r and \hat{u}_r gives the following equation for ω :

$$\begin{aligned}
 \rho_1^* A_1^2 f_2^0 + \rho_2^* A_2^2 f_1^0 \\
 - \frac{2i c_1 \rho^0 |u_1^0 - u_2^0|}{L} (A_1 f_2^0 + A_2 f_1^0) \\
 - k^2 \frac{2c_1 \rho^0 |u_1^0 - u_2^0|}{L} D^0 = 0.
 \end{aligned}$$

The solution to eqs. (A.1) and (A.2) is stable if $\text{Im}(\omega) \geq 0$. After some algebraic manipulation, it is found that this is satisfied for any value of k if,

$$D^0 \geq \frac{1}{2c_1} L |u_1^0 - u_2^0| / f_1^0 f_2^0. \tag{A.4}$$

For the steady-state problem, the turbulence kinetic equation gives

$$S_k = \epsilon,$$

i.e.

$$\frac{c_1 \rho^0 f_1^0 f_2^0}{L} |u_1^0 - u_2^0|^3 = \frac{0.09 \rho^0 k^{3/2}}{c_2 L},$$

whence

$$\begin{aligned}
 D^0 &= 2k^{1/2} l_t \\
 &= 2c_2 k^{1/2} L \\
 &= 2c_2 \left\{ \frac{c_1 c_2 f_1^0 f_2^0}{0.09} \right\}^{1/3} |u_1^0 - u_2^0| L.
 \end{aligned}$$

Hence condition (A.4) is satisfied for all f_r^0 if

$$c_1 c_2 > (0.09)^{1/4} / (4\sqrt{2}) = 0.1.$$

The preferred coefficient set (b) of section 5.2 has $c_1c_2 = 0.86$ for small density differences and $c_1c_2 = 0.60$ for large density differences. Hence for the simple situation considered here the turbulence model has stable solutions.

It is interesting to compare the results obtained here with the methods used by other authors to obtain an equation set with stable solutions. Two-pressure models have been widely used for this purpose; see, for example, Stuhmiller [23], Hancox et al. [24] and Ransom and Hicks [25]. In such models each fluid has its own pressure, p_r , and the pressure gradient term on the right-hand side of eq. (A.2) is modified as follows:

$$-f_r \frac{\partial p}{\partial x} \rightarrow -f_r \frac{\partial p_r}{\partial x} - (p_r - \hat{p}) \frac{\partial f_r}{\partial x}. \quad (\text{A.5})$$

\hat{p} denotes the interface pressure. In the present model, if the turbulent diffusion term is treated as a small correction, the drag on fluid 1 becomes

$$D_{12} \approx -\frac{c_1 f_1 f_2 \rho}{L} |u_1 - u_2| (u_1 - u_2) - \frac{2c_1 \rho}{L} |u_1 - u_2| D \frac{\partial f_1}{\partial x}.$$

Then if the limiting value (A.4) is used for D , the effect is to add the term

$$-\rho f_1 f_2 (u_1 - u_2)^2 \frac{\partial f_r}{\partial x}$$

to the right-hand side of (A.2). As in the two-pressure models a term proportional to the volume fraction gradient is introduced. The result obtained is similar to the two-pressure model given in [23, 24] for bubbly or droplet flow (f_1 small) which uses

$$p_1 = p_2 = p,$$

$$p - \hat{p} = c_p \rho_2 (u_1 - u_2)^2,$$

where c_p = dynamic pressure coefficient.

The pressure difference is derived by considering the flow past a sphere.

Hence the inclusion of turbulent diffusion terms as described in section 5.1, although obtained by very different physical reasoning, bears a strong resemblance to two-pressure models.

References

- [1] G.I. Taylor, The instability of liquid surfaces when accelerated in a direction perpendicular to their planes. I, Proc. Roy. Soc. A 201 (1950) 192.
- [2] D.H. Sharp, An overview of Rayleigh–Taylor instability, *Physica D* 12 (1984) 3.
- [3] M.H. Emery, J.P. Dahlburg and J.H. Gardner, The Rayleigh–Taylor instability in ablatively accelerated targets with 1, $\frac{1}{2}$ and $\frac{1}{4}$ μm laser light, *Phys. Fluids* 31 (1988) 1007.
- [4] R.D. Richtmyer, Taylor instability in shock acceleration of compressible fluids, *Commun. Pure Appl. Math.* 13 (1960) 297.
- [5] E.E. Meshkov, *Izv. Akad. Nauk. SSSR, Mekh. Zhidk. Gaza* 5 (1969) 151.
- [6] M. Brouillette and B. Sturtevant, Growth induced by multiple shock waves normally incident on plane gaseous interfaces, these Proceedings, *Physica D* 37 (1989) 248.
- [7] D. Besnard, J.F. Haas and R. Rauenzahn, Statistical modelling of shock–interface interaction, these Proceedings, *Physica D* 37 (1989) 227.
- [8] D.L. Youngs, Numerical simulation of turbulent mixing by Rayleigh–Taylor instability, *Physica D* 12 (1984) 19.
- [9] K.I. Read, Experimental investigation of turbulent mixing by Rayleigh–Taylor instability, *Physica D* 12 (1984) 45.
- [10] K.I. Read and D.L. Youngs, Experimental investigation of turbulent mixing by Rayleigh–Taylor instability, AWRE Report 0-11/83 (1983).
- [11] K.D. Burrows, V.S. Smeeton and D.L. Youngs, Experimental investigation of turbulent mixing by Rayleigh–Taylor instability, II, AWRE Report No. 0-22/84 (1984).
- [12] V.S. Smeeton and D.L. Youngs, Turbulent mixing by Rayleigh–Taylor instability, III, AWE Report No. 0-35/87 (1988).
- [13] B. van Leer, Towards the ultimate conservative difference scheme: IV, a new approach to numerical convection, *J. Comp. Phys.* 23 (1977) 276.
- [14] D.L. Youngs, Time-dependent multi-material flow with large fluid distortion, in: *Numerical Methods for Fluid Dynamics*, K.W. Morton and M.J. Baines, eds. (Academic Press, New York, 1982).
- [15] G. Tryggvason, Numerical simulations of Rayleigh–Taylor instability, *J. Comp. Phys.* 75 (1988) 253.
- [16] R.M. Kerr, Simulations of Rayleigh–Taylor flows using vortex blobs, *J. Comp. Phys.* 76 (1988) 48.
- [17] D.B. Spalding, A turbulence model for buoyant and combusting flows, *Int. J. Multiphase Flow* 24 (1987) 1.

- [18] M.J. Andrews, Turbulent mixing by Rayleigh–Taylor instability, Imperial College Report CFDU 86/10 (1986).
- [19] A.V. Jones and A. Prosperetti, On the suitability of first-order differential models for two-phase flow prediction, *Int. J. Multiphase Flow* 11 (1985) 133.
- [20] C.E. Leith, Coherent structures in a turbulence model with stochastic backscatter, unpublished.
- [21] B.E. Launder and D.B. Spalding, *Mathematical Models of Turbulence* (Academic Press, New York 1972).
- [22] J.R. Travis, F.H. Harlow and A.A. Amsden, Numerical calculation of two-phase flows, *Nucl. Sci. Eng.* 61 (1976) 1.
- [23] J.H. Stuhmiller, Influence of interfacial pressure forces on the character of two-phase flow model equations, *Int. J. Multiphase Flow* 3 (1977) 551.
- [24] W.I. Hancox, R.L. Ferch, W.S. Lui and R.E. Nieman, One-dimensional models for transient gas–liquid flows in ducts, *Int. J. Multiphase Flow* 6 (1979) 25.
- [25] V.H. Ransom and D.L. Hicks, Hyperbolic two-pressure models for two-phase flow, *J. Comp. Phys.* 53 (1984) 124.